Ouafa Hamidane[1,2,], Brahim Chermime[1], Mamoun Fellah[1], Mohamed Mounes Alim[3]*

[1]Faculty of Science and Technology, Department of Mechanical Engineering, University Abbes Laghrour,Khenchela, Algeria, [2]Advanced Materials Science and Engineering Laboratory ISMA, Khenchela, Algeria, [3]Center for the Development of Advanced Technologies (CDTA), City 20 August 1956, Baba Hassan, Algiers, Algeria

Scientific paper
ISSN 0351-9465, E-ISSN 2466-2585
https://doi.org/10.62638/ZasMat1668

Zastita Materijala 67 ()
(2026)

The impact of plasma nitriding bias voltages on mechanical characteristics of 25Cr2Ni4W steel

ABSTRACT

This study investigates the influence of negative bias voltage on the plasma nitriding behavior of 25Cr2Ni4W low-alloy steel to enhance its surface mechanical and tribological performance. The bias voltage was systematically varied from 2.0 to 3.5 kV, while discharge power, pressure, and treatment time were kept constant. Substrate heating was achieved through a self-induced mechanism. X-ray diffraction (XRD) analysis confirmed the formation of a compound layer consisting of ε-$Fe_{2-3}N$ and γ'-Fe_4N phases. With increasing bias voltage, a progressive transformation toward the γ'-Fe_4N phase was observed, accompanied by a reduction in ε-$Fe_{2-3}N$ content. This microstructural evolution significantly affected surface mechanical properties. Nanoindentation results revealed a marked increase in hardness compared with the untreated substrate. The sample treated at 2.0 kV (CW1) exhibited the highest and most stable nanohardness (≈ 6000 MPa), indicating a dense and coherent nitride layer. Conversely, the 3.5 kV (CW4) condition yielded a lower nanohardness (≈ 4000 MPa) due to excessive sputtering and reduced nitrogen diffusion. These results demonstrate that accurate control of negative bias voltage is a key factor in tailoring the nitride phase composition and optimizing surface hardening in plasma-nitrided 25Cr2Ni4W steel.

Key words: *Plasma nitriding, Low alloy steel, Nitride phases, Nano-hardness*

1. INTRODUCTION

The mechanical performance of engineering alloys is strongly influenced by both bulk composition and surface condition. Among these alloys, the low-alloy steel 25Cr2Ni4W has been widely adopted in the manufacturing of pipes, railroad tracks, automobile and aircraft bodies, as well as in onshore and offshore structural engineering, owing to its high strength and toughness. Alloying elements such as chromium, molybdenum, and vanadium contribute to enhanced hardenability, corrosion resistance, and fatigue strength. [1].

However, despite these advantages, 25Cr2Ni4W may still experience performance limitations under severe wear, cyclic loading, or impact conditions [2] [3]. These challenges have motivated the development and application of advanced surface engineering techniques to further improve its service life and reliability [4].

*Corresponding author:Ouafa Hamidane
E-mail: ouafa.hamidane@univ-khenchela
Paper received: 12.12.2025.
Paper corrected: 24.02.2026.
Paper accepted: 28.03.2026.

Thermochemical surface treatments are widely applied to extend component life by improving hardness [5], wear resistance, and fatigue strength [6-8]. Plasma nitriding (ion nitriding) is particularly effective because it forms hardened surface layers while preserving the material's core properties [9,10]. Owing to this balance, it is extensively used in the automotive, aerospace, and tooling industries [11,12].

Plasma nitriding relies on the diffusion of nitrogen into the metallic substrate at temperatures between 350–600 °C, forming a hardened compound layer and diffusion zone [13,14]. This process increases fatigue resistance and wear performance while allowing for controlled property tailoring [15].

The treatment is performed in a low-pressure chamber containing nitrogen-based gases such as ammonia or nitrogen–hydrogen mixtures. An electrical discharge generates plasma, ionizing the gas [16]. The positively charged nitrogen ions are accelerated toward the negatively biased specimen surface, where they are absorbed and diffuse into the lattice [17,18]. Despite its advantages of uniformity and precision, plasma nitriding requires careful process control to avoid excessive brittleness [19].

Nitrogen uptake during treatment occurs via sputtering, adsorption, and diffusion, leading to the formation of a compound (white) layer and a diffusion zone [20,21]. These modified layers significantly affect mechanical behavior, particularly fracture toughness and impact resistance [22]. Optimizing the treatment parameters is therefore critical for achieving the desired property balance [23].

This study examines the influence of plasma nitriding on the impact toughness of Charpy test specimens. [24,25]. By correlating nitriding parameters such as temperature, duration, and gas composition with impact energy absorption [26]. This work provides new insights into the relationship between surface hardening and toughness [27]. These findings are especially relevant to applications where components must withstand sudden impact and cyclic stresses [28].

2. EXPERIMENTALPART

2.1. Materials

The chemical composition of this low-alloy steel is presented in Table 1. The presence of nickel and chromium enhances the tensile strength, wear resistance, and ductility of 25Cr2Ni4W, while manganese improves its hardenability [29].

Table 1. Chemical composition of low-alloyed steel

Elements	C %	Mn	Cr	Ni	W	P	S
Wt[%]	0.28	0.5	1.5	3.97	0.73	0.02	0.01

In this study, cylindrical samples of 25Cr2Ni4W (diameter: 22 mm, thickness: 10 mm) were supplied by ECMK Company located in Khenchela-Algeria. Prior to treatment, the flat surfaces were mirror-polished using SiC sandpapers with grit sizes of 180, 320, 600, 800, 1000, and 1400 in sequential order (Struers, Ballerup, Denmark).

Subsequently, the samples were further polisheusing a disk polishing machine with a 3 µm diamond paste (Struers, Ballerup, Denmark). Finally, a chemical etching process was performed using a solution of 4% nitric acid (Sigma-Aldrich, St. Louis, MO, USA) in 96% ethanol (Merck, Darmstadt, Germany) to thoroughly cleanse the samples and remove any residual contaminants.

2.2. Plasma nitriding processing

The plasma nitriding experiments were carried out in a spherical chamber with a diameter of 930 mm, equipped with a vacuum system capable of achieving a base pressure of 10^{-3}mTorr. Initial evacuation was performed using a primary pump reaching ~1 mTorr, followed by a secondary oil diffusion pump to obtain the higher vacuum level. An inductively coupled plasma (ICP) source, fabricated in-house, was energized by a 13.56 MHz RF generator through a surrounding copper coil.

Figure1. System of plasma nitriding

The ICP source measures 170 mm in length, 100 mm in diameter, and 5 mm in thickness. Samples were mounted on a 1500 mm long, 13 mm diameter quartz substrate holder, chosen for its insulating properties to minimize electrical breakdown and arcing under DC bias. A high-voltage DC power supply (model HCN 2800–6500, CDTA Laboratory, Algiers, Algeria) was used to bias the specimens at 400 mA/6.5 kV or higher. The sample-to-plasma source distance was fixed at 100 mm in all treatments to ensure uniform surface modification. As shown in Table 2, three specimens (CW1, CW2, and CW3) were plasma nitrided under identical treatment conditions of discharge power (200 W), chamber pressure (60 mTorr), and duration (90 min).

Table 2. Experimental parameters

Samples	Parameters
CW1	Biased voltage **2.0 kV,** Discharge power = 200 W Pressure = 60 mTorr t = 90 min
CW2	Biased voltage **2.5 kV,** Discharge power = 200W Pressure = 60 mTorr t = 90 min
CW3	Biased voltage **3.0 kV,** Discharge power = 200W Pressure = 60 mTorr t = 90 min
CW4	Biased voltage **3.5KV,** Discharge power = 200 W Pressure = 60 mTorr t = 90min

The only variable parameter was the applied negative bias voltage, which was set to 2.0 kV, 3.0 kV, and 3.5 kV for CW1, CW2, and CW3, respectively. This experimental design isolates the effect of bias voltage on nitrogen ion bombardment energy, thereby influencing nitrogen uptake, diffusion depth, and the formation of the nitrided layer. Consequently, a comparative analysis of the three samples provides insight into the relationship between ion acceleration energy and the resulting mechanical and microstructural properties of the treated material.

3. RESULTS AN DDISCUSSION

3.1 X-ray diffraction analysis

Figure 2 presents the XRD diffractograms of the developed samples. For the CW1 sample, exposed to a polarization voltage of 2.0 KV, three peaks at 40.3°, 44.9°, and 81.75° can be identified. The first peak is associated with ε-$Fe_{2-3}N$, while the remaining peaks can be assigned to α-Fe. The XRD diffractograms of the samples treated at 3.0 kV and 3.5 kV still exhibit peaks related to these phases, but the intensity of the peak at 44.9° has significantly decreased.

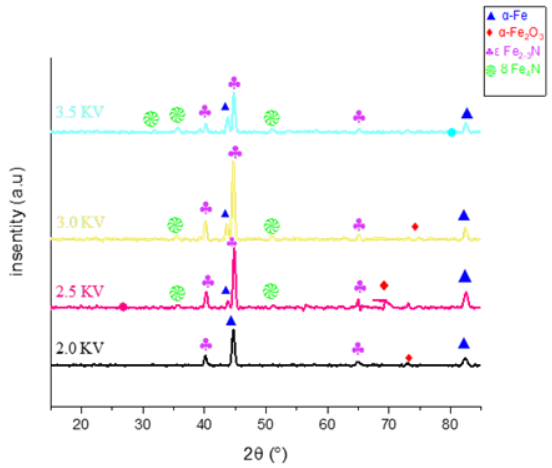

Figure 2. XRD diffraction patterns of CW1, CW3 and CW4 samples.

The γ'-Fe_4N phase has been identified as the source of the weak peaks, located approximately at 35.7° and 51.8°, in the XRD diagram of the sample treated at 3.0 kV, CW2. Additionally, another weak-intensity peak appears at 65.6°, attributed to the ε-$Fe_{2-3}N$ phase. According to Vegard's law [27], this is likely due to a reduction in nitrogen content, modifying the lattice parameter of the ε-$Fe_{2-3}N$ phase. A low-intensity peak at 58.7° for the 3.5 kV-treated sample, CW3, is identified and associated with the α-Fe_2O_3 phase. These observations can be explained by greater self-heating at 3.5 kV compared to 3.0 kV, leading to enhanced nitrogen diffusion but a lower nitrogen concentration in the treated layers of the sample. The presence of the γ'-Fe_4N phase at 3.5 kV can be attributed to diffusion phenomena, resulting in increased nitrogen penetration. These findings are consistent with the binary phase diagram of the Fe-N system [28], indicating the presence of the ε-$Fe_{2-3}N$ and γ'-Fe_4N phases.

The crystallite size was estimated from the XRD patterns using the Scherrer equation:

$$D = \frac{K.\lambda}{\beta.\cos\theta}$$

In the table 3 the results reveal a clear dependence on the applied bias voltage during plasma nitriding.

Table 3.TheCristallite size of the three treated samples

Sample ID	Peak Position (2θ, °)	FWHM (β, rad)	Crystallite Size, D (nm)
CW1	40.17842	0.40465	21.85
	44.70079	0.42984	20.89
	64.99936	0.54973	17.91
	73.06546	0.43035	24.01
	82.4015	0.58467	18.88
	D moy = 20.7		
CW2	35.7067	0.45975	18.98
	40.28501	0.39186	22.57
	42.16998	0.34802	25.57
	44.84471	0.39062	23.00
	51.21551	0.41668	22.10
	64.96174	0.25376	38.79
	69.6938	0.6604	15.32
	82.52233	0.59849	18.46
	D moy = 23.1		
CW3	35.45618	0.39669	21.98
	40.1710	0.37298	23.71
	43.67256	0.38056	23.51
	44.70088	0.40489	22.17
	51.00606	0.42115	21.85
	65.07635	0.36353	27.10
	73.09938	0.34741	29.75
	82.44559	0.47556	23.21
	D moy = 24.16		
CW4	31.927	0.27958	30.89
	35.65299	0.41045	21.25
	40.24958	0.32835	26.93
	43.76197	0.40573	22.06
	44.79635	0.39436	22.77
	50.98864	0.4132	22.26
	65.13064	0.37369	26.37
	82.518140	0.47564	23.22
	D moy = 24.46		

At 2.0 kV, the crystallite sizes are relatively small, ranging from 22 to 29 nm, with an average of 24.68 nm, indicating limited grain growth and a predominantly fine microstructure. At 3.0 kV, crystallite sizes increase to 36–49 nm (average 41.21 nm), suggesting enhanced nitrogen diffusion and crystallite coalescence. The effect is most pronounced at 3.5 kV, where crystallite sizes range from 29 to 90 nm (average 57.54 nm), reflecting substantial grain growth under high-energy ion bombardment. This progressive increase in crystallite size with bias voltage highlights the strong influence of processing parameters on microstructural evolution: while low voltages preserve fine grains beneficial for hardness, higher voltages favor larger crystallites that may improve toughness but reduce surface hardness uniformity.

Figure 3 illustrates the evolution of indentation hardness as a function of cycle number for plasma-nitrided25Cr2Ni4W steel treated under different bias voltages (CW1–CW4). All samples exhibit a rapid hardness increase during the first few cycles, corresponding to strain accumulation and work hardening at the surface due to cyclic plastic deformation. Thereafter, the hardness stabilizes, indicating a dynamic equilibrium between dislocation generation and recovery mechanisms within the nitrided layer.

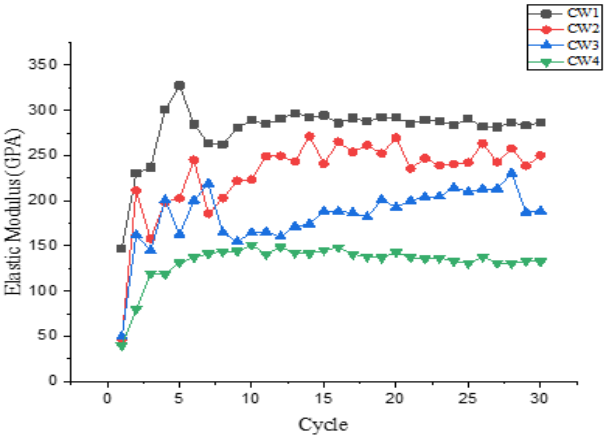

Figure 3. the evolution of indentation hardness as a function of cycle number.

The CW1 specimen, processed at the lowest bias voltage, presents the highest and most stable hardness values (≈6000 MPa), suggesting the development of a dense and fine nitride structure with uniform nitrogen diffusion. This behavior reflectsthe dominance of coherent γ′-Fe_4N and ε-$Fe_{2-3}N$ phases that effectively impede dislocation motion.

CW2 and CW3, treated at intermediate voltages, show slightly reduced hardness (≈5500 MPa and ≈5000 MPa, respectively) and minor cyclic fluctuations associated with localized stress relaxation and microstructural rearrangement.

Conversely, CW4, subjected to the highest bias voltage, displays the lowest hardness (~4000 MPa) and rapid stabilization. This reduction is attributed to excessive thermal effects causing grain coarsening and possible nitride over-saturation, which diminish matrix coherence and mechanical integrity.

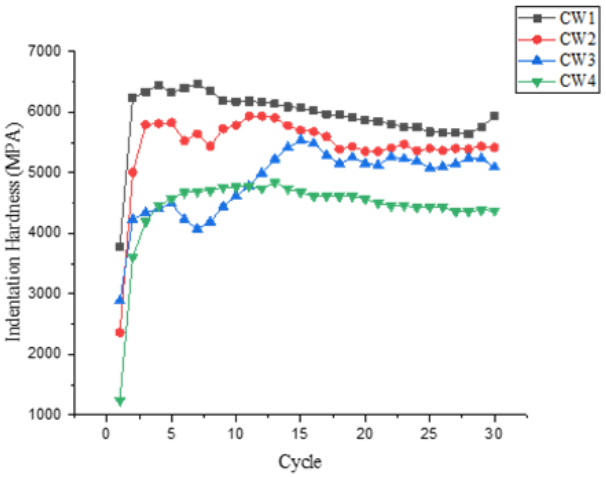

Figure 4. The variation of elastic modulus as a function of cycle number.

Figure 4 illustrates the variation of elastic modulus as a function of cycle number for plasma-nitrided 25Cr2Ni4W steel treated under different bias voltages (CW1–CW4).

The CW1 specimen, treated at the lowest bias voltage, achieves the highest modulus (~320 GPa), signifying a dense and coherent nitride structure that enhances elastic recovery. CW2 and CW3 show slightly lower moduli (~280 GPa and ~240 GPa, respectively), suggesting moderate lattice distortions and residual stress relaxation due to increased ion bombardment energy. Conversely, CW4, processed at the highest bias voltage, displays the lowest modulus (~200 GPa) and rapid stabilization, indicating microstructural coarsening and reduced lattice coherence caused by excessive thermal exposure.

These results confirm that increasing bias voltage beyond an optimal range adversely affects the elastic rigidity of the nitrided layer. Controlled bias conditions therefore favor the formation of fine, defect-free nitride phases, improving the elastic and mechanical stability of plasma-nitrided25Cr2Ni4W steel.

Figure 5 presents the variation of elastic energy with the number of cycles for plasma-nitrided 25Cr2Ni4W steel treated under different bias

voltages (CW1–CW4). A progressive increase in elastic energy is observed for all specimens, reflecting the accumulation of recoverable strain energy as the surface layer undergoes repeated elastic–plastic deformation. This trend signifies the enhancement of energy absorption capability due to cyclic stress-induced hardening.

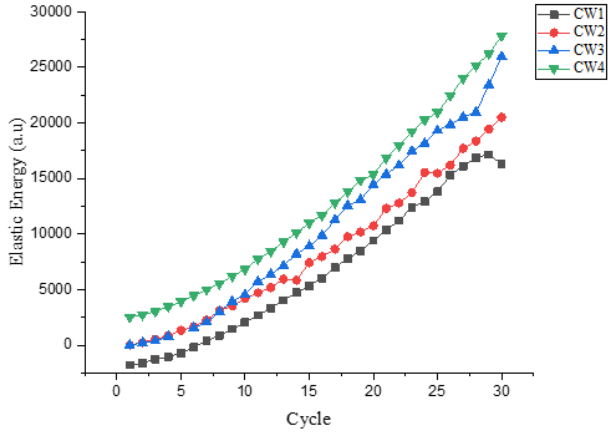

Figure 5. The variation of elastic energy with the number of cycles number.

Among the tested samples, CW4 processed under the highest bias voltage—exhibits the greatest elastic energy accumulation, reaching nearly 28,000 a.u. after 30 cycles. This behavior indicates a thicker diffusion zone and higher strain accommodation capacity, despite its lower hardness. CW3 and CW2 follow with intermediate values, while CW1, treated at the lowest bias voltage, shows the smallest energy accumulation, consistent with its more rigid and less deformable surface layer.

The gradual divergence among the curves suggests that higher bias voltages promote increased lattice strain and dislocation mobility within the nitrided region. However, excessive bias may also induce structural relaxation and microcrack initiation at longer cycles. Overall, the elastic energy evolution confirms that increasing bias voltage enhances the capacity of the nitrided layer to store and dissipate mechanical energy, up to an optimal level beyond which surface degradation may occur.

Figure 6 illustrates the evolution of plastic energy accumulation as a function of cycle number for plasma-nitrided25Cr2Ni4W steel treated under distinct DC bias voltages: CW1 (2.0 kV), CW2 (2.5 kV), CW3 (3.0 kV), and CW4 (3.5 kV). A pronounced and direct correlation is observed between increasing bias voltage and the exponential growth of accumulated plastic energy, indicating that higher electric fields substantially intensify fatigue-induced plastic deformation.

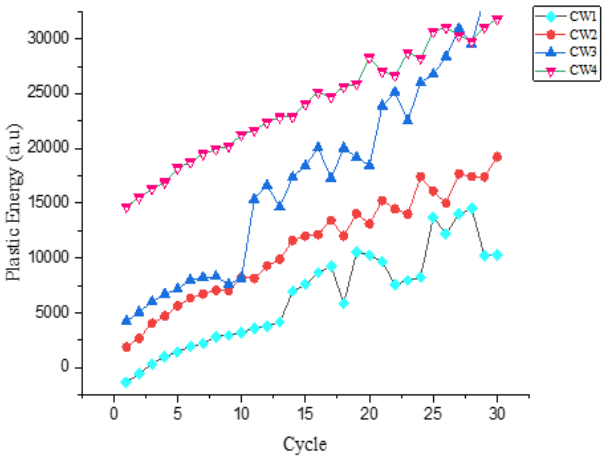

Figure 6.The evolution of plastic energy accumulation as a function of cycle number.

At lower voltages (2.0–2.5 kV), the plastic energy in CW1 and CW2 increases gradually, reflecting intermittent deformation mechanisms such as microcrack initiation, slip band evolution, or localized dislocation activity that activate only beyond specific energy thresholds. Conversely, at higher voltages (3.0–3.5 kV), specimens CW3 and CW4 exhibit markedly greater plastic energy accumulation, with CW4 displaying an almost linear, high-rate increase—characteristic of accelerated, continuous damage evolution. This suggests that elevated bias voltages enhance atomic mobility and reduce the activation barrier for dislocation motion, leading to intensified plastic flow and early fatigue damage.

4. CONCLUSIONS

The present study demonstrates that plasma nitriding is an effective method for improving the surface integrity of 25Cr2Ni4W low-alloy steel. The variation in negative bias voltage strongly influences the phase composition, microstructure, and mechanical response. XRD and nanoindentation analyses revealed that applying a lower bias voltage of 2.0 kV produces a dense and coherent nitride layer dominated by γ′-Fe_4N, resulting in the highest nanohardness (~6000 MPa) and elastic modulus (~320 GPa). In contrast, excessive ion energy at 3.5 kV promotes microstructural coarsening and reduces both hardness and modulus due to over-sputtering and thermal effects. The elastic–plastic energy analysis further confirmed that higher bias voltages enhance energy absorption but increase plastic deformation and potential fatigue susceptibility.

In addition, the formation of a compound layer consisting of ε-$Fe_{2-3}N$ and γ′-Fe_4N phases may also significantly influence the corrosion resistance

of the treated steel, although this aspect was not investigated in the present work.

Overall, these results highlight that maintaining a moderate negative bias voltage is essential for achieving optimal mechanical stability and surface hardening. Future investigations should focus on refining plasma parameters, exploring alternative alloy systems, and evaluating both the long-term tribological performance and corrosion behavior of nitrided components under actual service conditions.

5. REFERENCES

[1] M. Drouet, E. Le Bourhis(2023) “Low-Temperature Nitriding of Metal Alloys for Surface Mechanical Performance,” *Materials*, 16(13), 4704, doi: 10.3390/ma16134704

[2] Z. He, W. Wei, J. Hu, J. Gu, “Aluminum-Modified Plasma Nitriding with High Efficiency and Enhanced Performance,” *Coatings*, 14(11), 1373, 2024, doi: 10.3390/coatings14111373

[3] S. Satbayeva, et al. (2024) “Electrolytic Plasma Nitriding of Medium-Carbon Steel 45 for Performance Enhancement,” Crystals, 14(10), 895, doi: 10.3390/cryst14100895

[4] Y. He, et al. (2024) “Effect of Post-Plasma Nitrocarburized Treatment on Mechanical Properties of Carburized and Quenched 18Cr2Ni4WA Steel,” Lubricants, 12(5), 153, doi: 10.3390/lubricants12050153

[5] C. A. K. Reddy (2022) “Effect of Plasma Nitriding on M50NiL Steel—A Review,” Fisheries Science, 32(1), 804, doi: 10.2331/suisan.32.804

[6] Z. He, et al. (2024) “The Effect of Heat Treatment on the Plasma Nitriding of Hot-Rolled 17-7 PH Steel,” Metals, 14(6), 1061, doi: 10.3390/met14091061

[7] M. Mokrzycka (2024) “The Influence of Plasma Nitriding Process Conditions on the Nitride Layer and Properties,” Rzeszow University of Technology, 1, 1, doi: 10.7862/rm.2024.1

[8] V. Niksefat (2025) “Effect of Plasma Nitriding Duration on Tribological Performance,” Journal of Materials Research and Technology, 34, 102540, doi: 10.1016/j.jmrt.2024.12.261

[9] M. Hirano (2025) “Hydrogen-Free Plasma Nitriding Process for Fabrication of Expanded Austenite,” Materials, 18(1), 140, doi: 10.3390/ma18010140

[10] Ž. Stojanović (2025) “Decarburization and Its Effects on the Properties of Plasma-Nitrided Steels,” Materials, 18(10), 2207, doi: 10.3390/ma18102207

[11] U. Ratayski (2022) “Influence of Elevated Temperature and Reduced Pressure on Nitriding,” Engineering Reports, 4(12), e12371, doi: 10.1002/eng2.12371

[12] K. Lin (2023) “Active Screen Plasma Nitriding of LPBF and Forged 316L Stainless Steel,” Surface Engineering, 39(4), 456-465, doi: 10.1080/17452759.2023.2225490

[13] S. O. Chong, S. J. Kim (2019) “Effects of Molybdenum on Improvement of Anti-Corrosion by Plasma Ion Nitriding for Austenitic Stainless Steels,” J. Nanosci. Nanotechnol., 19(4), 2198–2201, doi: 10.1166/jnn.2019.16006.

[14] T. Bell et al. (2023) “Ion/Plasma NitridingVersus Gas Nitriding,” Materialwiss. Werkstofftech., 54(5), 580–592, doi: 10.1002/mawe.202300067.

[15] H. J. Spies, A. Dalke (2019) “Low-Temperature Plasma Nitriding of Low-Alloy Steel for Hardness Improvement,” Materialwiss. Werkstofftech., 50(3), 241–252, doi: 10.1002/mawe.201900012.

[16] I. Braceras (2025) “Plasma-NitridedFerritic Stainless Steel as Hydrogen Diffusion Barrier,” Surf. Coat. Technol., 490, 131902, doi: 10.1016/j.surfcoat.2025.131902.

[17] S. O. Chong, L. Shao, F. A. Garner (2024) “Advanced cathodic cage plasma nitriding for corrosion resistance of nuclear reactor cladding materials,” Surface and Coatings Technology, 485, 130448, doi: 10.1016/j.surfcoat.2024.130448.

[18] Y. Wang et al. (2020) “Plasma Nitriding Effects on Low Alloy Cr-Mo-V Steels,” Surf. Coat. Technol., 385, 125450, doi: 10.1016/j.surfcoat.2020.125450.

[19] N. K. Krioni et al. (2024) “Study of Wear Resistance of Plasma NitridedGGG60 Using Response Surface Methodology,” J. Frict. Wear, 45(1), 55–62, doi: 10.3103/s1068366625700035.

[20] O. Hamidane (2024) “Study of the Mechanical and TribologicalBehaviour of a Low-Alloy Steel Treated by Nitriding,” Seven Editora, 5(3), 74–85, doi: 10.54021/seesv5n3-074.

[21] B. Venkatesh et al. (2024) “Changes of Structure and Properties in Alloy Steels Thermochemically Treated by Plasma Nitriding,” Bohrium Publ., 2(1), 12–24, doi: 10.2139/ssrn.4705126.

[22] E. Rolinski, M. Woods (2022) “Plasma Nitriding as a Low-Nitriding Potential Process,” Therm. Process. Mag., 11(12), 24–29.

[23] C. A. K. Reddy et al. (2022) “Influence of Plasma Nitriding Parameters on Layer Thickness and Compound Layer Formation,” Eng. Rep., 4(12), e12371, doi: 10.1002/eng2.12371.

[24] J. Baranowska (2022) “Impact of Nitriding Parameters on Properties of Stainless Steel Plasma-Nitrided in Glow Discharge,” Vacuum, 195, 110680, doi: 10.1016/j.vacuum.2021.110680.

[25] K. Miyamoto, Y. Yoshida (2023) “Surface Modification of AISIH13 Tool Steel via Atmospheric-Pressure Plasma Nitriding and Steam Treatment,” ISIJ Int., 64(1), 92–101, doi: 10.2355/isijinternational.ISIJINT-2023-289.

[26] M. Hirano et al. (2020) “Low-Temperature Plasma Nitriding for Expanded Austenite in Laser-Deposited Alloys,” Materials, 13(1), 140, doi: 10.3390/ma13010140.

[27] C. A. K. Reddy et al. (2024) “Influence of Plasma Nitriding on Surface Layer of M50NiL Steel,” J. Mech. Behav. Mater., 33(1), 20240022, doi: 10.1515/jmbm-2024-0022.

[28] B. Venkatesh et al. (2025) “Comparison of Nitriding Processes for M50NiL—Gas vs Plasma vs Liquid,” Arch. Metall. Mater., 70(1), 105–117, doi: 10.24425/amm.2025.150471.

[29] A. Horton (2014) “Zinc Metallizing for External Corrosion Control of Ductile Iron Pipe,” Pipelines ,p.1307–1318, doi: 10.1061/9780784413692.120.

IZVOD

UTICAJ NAPONA PREDNAPONA PLAZMA NITRIRANJA NA MEHANIČKE KARAKTERISTIKE ČELIKA 25CR2NI4W

Ova studija istražuje uticaj negativnog napona prednapona na ponašanje plazma nitriranja niskolegiranog čelika 25Cr2Ni4W kako bi se poboljšale njegove površinske mehaničke i triboloških performanse. Napon prednapona je sistematski varirao od 2,0 do 3,5 kV, dok su snaga pražnjenja, pritisak i vreme obrade održavani konstantnim. Zagrevanje podloge je postignuto samoindukovanim mehanizmom. Analiza rendgenske difrakcije (XRD) potvrdila je formiranje složenog sloja koji se sastoji od faza e-$Fe_{2-3}N$ i g'-Fe_4N. Sa povećanjem napona prednapona, primećena je progresivna transformacija ka fazi g'-Fe_4N, praćena smanjenjem sadržaja e-$Fe_{2-3}N$. Ova mikrostrukturna evolucija značajno je uticala na mehanička svojstva površine. Rezultati nanoindentacije otkrili su značajno povećanje tvrdoće u poređenju sa neobrađenom podlogom. Uzorak tretiran na 2,0 kV (CW1) pokazao je najveću i najstabilniju nanotvrdoću (≈ 6000 MPa), što ukazuje na gust i koherentan nitridni sloj. Nasuprot tome, uslov od 3,5 kV (CW4) dao je nižu nanotvrdoću (≈ 4000 MPa) zbog prekomernog raspršivanja i smanjene difuzije azota. Ovi rezultati pokazuju da je precizna kontrola negativnog napona prednapona ključni faktor u prilagođavanju sastava nitridne faze i optimizaciji površinskog očvršćavanja plazma nitridiranog čelika 25Cr2Ni4W.

***Ključne reči**: Plazma nitriranje, niskolegirani čelik, nitridne faze, nanotvrdoća*

Naučni rad
Rad primljen: 12.12.2025.
Rad korigovan: 24.2.2026.
Rad prihvacen: 28.03.2026.

OuafaHamidane: 0009-0007-0263-7071
ChermimeBrahim: 0000-0002-2399-4779
Mohamed MounesAlim: 0000-0002-0624-3113
Mamoun Fellah: 0000-0003-0615-6711